

Research Articles: Systems/Circuits

Encoding of environmental cues in central amygdala neurons during foraging

<https://doi.org/10.1523/JNEUROSCI.1791-21.2022>

Cite as: J. Neurosci 2022; 10.1523/JNEUROSCI.1791-21.2022

Received: 1 September 2021

Revised: 3 February 2022

Accepted: 8 March 2022

This Early Release article has been peer-reviewed and accepted, but has not been through the composition and copyediting processes. The final version may differ slightly in style or formatting and will contain links to any extended data.

Alerts: Sign up at www.jneurosci.org/alerts to receive customized email alerts when the fully formatted version of this article is published.

1 **Encoding of environmental cues in central amygdala neurons during foraging**

2 **Marion Ponserre^{1*}, Federica Fermani^{1*}, Louise Gaitanos¹ and Rüdiger Klein¹**

3 1 Max-Planck Institute of Neurobiology, Department of Molecules – Signaling – Development, 82152
4 Martinsried, Germany.

5 * These authors contributed equally to this work

6 Correspondence should be addressed to Rüdiger Klein at rklein@neuro.mpg.de.

7 **Abbreviated title:** Contextual memories in CeA neurons

8 **Keywords:** Central amygdala, reward learning, foraging, associative memory, optogenetic, miniscope
9 calcium imaging

10 Number of pages: 40

11 Number of Figures: 6 main figures and 1 extended

12 Number of tables: 0

13 Number of words for Abstract: 158

14 Number of words for Introduction: 469

15 Number of words for Discussion: 888

16 **Conflicts of interest:**

17 The authors declare no competing financial interests.

18 **Acknowledgments:**

19 We thank Nejc Dolensek, Aljoscha Leonhardt, Matthias Meier, and Ruben Portugues for their help with
20 data analysis. We thank J. Cotino and Y. Pignot for their help with management of the animal colony. This
21 study was supported by the Max-Planck Society, the Deutsche Forschungsgemeinschaft (SPP1665), the
22 European Research Council under the European Union's Horizon 2020 research and innovation
23 programme (No. 885192).

24 **Abstract**

25 In order to successfully forage in an environment filled with rewards and threats, animals need to rely on
26 familiar structures of their environment that signal food availability. The central amygdala (CeA) is known
27 to mediate a panoply of consummatory and defensive behaviors, yet how specific activity patterns within
28 CeA subpopulations guide optimal choices is not completely understood. In a paradigm of appetitive
29 conditioning in which mice freely forage for food across a continuum of cues, we found that two major
30 subpopulations of CeA neurons, Somatostatin-positive (CeA^{Sst}) and protein kinase C δ -positive (CeA^{PKC δ})
31 neurons can assign motivational properties to environmental cues. While the proportion of food
32 responsive cells was higher within CeA^{Sst} than CeA^{PKC δ} neurons, only the activities of CeA^{PKC δ} , but not CeA^{Sst},
33 neurons were required for learning of contextual food cues. Our findings point to a model in which CeA^{PKC δ}
34 neurons may incorporate stimulus salience together with sensory features of the environment to encode
35 memory of the goal location.

36 **Significance Statement**

37 The CeA has a very important role in the formation of memories that associate sensory information with
38 aversive or rewarding representation. Here, we used a conditioned place preference paradigm, where
39 freely moving mice learn to associate external cues with food availability, to investigate the roles of CeA
40 neuron subpopulations. We found that CeA^{Sst} and CeA^{PKC δ} neurons encoded environmental cues during
41 foraging but only the activities of CeA^{PKC δ} neurons were required for learning of contextual food cues.

42 Introduction

43 An organism's survival depends heavily on its ability to evaluate whether familiar cues in the environment
44 predict a threat or an opportunity. The CeA is important for this competence and contains numerous
45 genetically distinct subpopulations of neurons that can select the appropriate behavioral outputs in the
46 face of positively or negatively valenced stimuli (Ehrlich et al., 2009; Pare and Duvarci, 2012; Herry and
47 Johansen, 2014; Janak and Tye, 2015; Fadok et al., 2018). While earlier models interpreted the literature
48 in a binary mode, where CeA neurons belong either to the "aversive" or "rewarding" network, new
49 hypotheses depict the CeA as an essential site for associative learning (Wilensky et al., 2006; Ciochi et
50 al., 2010) also contributing to the computation of prediction error signals (Ozawa et al., 2017; Yu et al.,
51 2017; Kargl et al., 2020). To understand how the surrounding environment modulates plasticity in CeA
52 circuits to drive behavioral selection, we probed the function and activity patterns of CeA^{PKC δ} and CeA^{Sst}
53 neurons during a foraging task. PKC δ - and Sst-expressing cells represent two non-overlapping populations
54 of CeA neurons (Kim et al., 2017), encompassing the majority of all cells in this region (Kim et al., 2017),
55 and are known to mediate antagonizing behaviors when studied in parallel (Kim et al., 2017; Wilson et al.,
56 2019; Kargl et al., 2020). The CeA has been previously shown to acquire responses to signals of food
57 delivery, but the contribution of these two CeA subpopulations has remained unclear (Gallagher et al.,
58 1990; Han et al., 1997, 1999; McDannald et al., 2004; Corbit and Balleine, 2005; Lee et al., 2005). In
59 particular, how these appetitive memories are represented in a setting where the animal freely navigates
60 and is forced to engage goal-oriented actions remains unknown. We hypothesized that PKC δ + cells that
61 integrate convergent inputs from cortical, thalamic, hippocampal, and brainstem structures (Douglass et
62 al., 2017), properties that are reminiscent of the Hebbian model of learning-induced synaptic plasticity,
63 may be involved in associative learning tasks that impose valence on different tastes or link taste valence
64 to other sensory stimuli.

65 Indeed, we found that CeA^{PKC δ} neurons, previously related to aversive behavior (Haubensak et al., 2010;
 66 Cai et al., 2014; Cui et al., 2017; Kim et al., 2017; Yu et al., 2017; Wilson et al., 2019), were required for
 67 approach behavior in a context that signals food availability, whereas CeA^{Sst} neurons were not. We
 68 performed Ca²⁺ imaging to evaluate neuronal activity changes when the mice freely decided to switch
 69 between environments. We observed that after learning, a subset of these two populations had
 70 developed specific activities to the positive context. Our findings suggest a model in which CeA^{Sst} neuron
 71 activity encodes information directly related to food consumption, whereas CeA^{PKC δ} cells endow sensory
 72 features of the environment with representation of the food reward salience to ultimately drive correct
 73 behavioral choices.

74 **Materials and Methods**

75 **Animals**

76 Prkcd-Cre (Tg(Prkcd-glc-1/CFP,-Cre)EH124Gsat) BAC mice were imported from the Mutant Mouse
 77 Regional Resource Center. Sst-Cre (Ssttm2.1(cre)Zjh) transgenic mice were acquired from the Jackson
 78 Laboratory (<https://www.jax.org/>). Rosa26R Cre dependent reporter mice that express LacZ (B6.129S4-
 79 Gt(ROSA)26Sortm1Sor/J) have been described previously (Soriano, 1999). Mice were backcrossed onto a
 80 C57BL/6NRj background (Janvier Labs - <http://www.janvier-labs.com>). 3-6 month old male Prkcd-cre;LacZ
 81 or Sst-Cre;LacZ mice were used for the place preference assay combined with optogenetic manipulation
 82 of CeA^{PKC δ} and CeA^{Sst} cells, as well as for the open field task. 8 to 18 month old male and female Prkcd-
 83 cre;LacZ or Sst-Cre;LacZ mice were used for the place preference assay combined with Ca²⁺ imaging of
 84 CeA^{PKC δ} and CeA^{Sst} cells. The older age of mice used for the Ca²⁺ imaging experiments was primarily due
 85 to the experimental design. In some cases, a waiting period of several months was necessary for the
 86 inflammation to decrease and to clearly see fluorescent cells through the lens. Mice were kept on a 12-h

light/dark cycle. All behavior experiments were conducted during the light phase of the cycle and under dimmed light in the behavioral boxes.

Viral Constructs

The following AAV viruses were purchased from the University of North Carolina Vector Core (<https://www.med.unc.edu/genetherapy/vectorcore>): AAV5-ef1a-DIO-eNpHR3.0-mCherry, AAV5-ef1a-DIO-mCherry. The AAV5-Syn.Flex.GCaMP6s virus was obtained from Addgene (<http://www.addgene.org/>).

Stereotaxic surgeries

Viral injections in the CeA

Mice were anaesthetized using isoflurane (Cp-Pharma) (induction, 3%; maintenance, 1.5%) in oxygen-enriched air and head-fixed on a stereotaxic frame (Model 1900 – Kopf Instruments). Body temperature was maintained at 37°C using a heating pad. Carprofen (Rimadyl – Zoetis) (5 mg/kg body weight), and an analgesic, were given via subcutaneous injection. Mice were bilaterally injected with 0.3 µl of virus in the CeA by using the following coordinates calculated with respect to the bregma: –1.22 mm anteroposterior, ± 2.9 mm lateral, –4.7 to –4.8 mm ventral. Viral particles were delivered using glass pipettes (708707 - Blaubrand intraMark) connected to a Picospritzer III (Parker Hannifin Corporation) and controlled by a Master-8 pulse stimulator (A.M.P.I) at a flow rate of ~50 nL/min. After delivery of the virus, the pipette remained in the brain for 5 min to prevent spread of the virus. Virus was allowed to be expressed for a minimum duration of 4.5 weeks and a maximum of 10 weeks before behavioral experiments.

Optic fibers implants

Mice used in optogenetic experiments were, in the same surgery, bilaterally implanted with optic fibers (200-µm core, 0.22 NA, 1.25-mm ferrule - Thorlabs) above the CeA (–4.35 mm ventral from bregma). The

109 skull was first protected with a thin layer of histo glue (Histoacryl, Braun), the fibers were then fixed to
110 the skull using UV light-curable glue (Loctite AA3491 - Henkel), and the exposed skull was covered with
111 dental acrylic (Paladur - Heraeus).

112 GRIN lens implantation and baseplate fixation.

113 For gradient index (GRIN) lenses implantation, 3 weeks after viral injection, mice expressing GCaMP6s in
114 PKC δ + or SST+ cells were anesthetized using the same procedure as described above. A small craniotomy
115 was made above the CeA using the same coordinates as for the injection of the viral preparation. Debris
116 were removed from the hole and a customized blunted 23G needle (0.7mm in diameter) was slowly
117 lowered down into the brain at a speed of 150 μ m/min to a depth of -4.6 mm from bregma. After
118 retraction of the needle, a GRIN lens (ProView Lens; diameter, 0.5 mm; length, ~8.4 mm, Inscopix)
119 mounted on a GRIN lens-holder was slowly (150 μ m/min) implanted above the CeA. The skull was first
120 protected with a thin layer of histo glue (Histoacryl, Braun), the lens was then fixed to the skull using UV
121 light-curable glue (Loctite AA3491 - Henkel), and the exposed skull was covered with dental acrylic
122 (Paladur - Heraeus). The exposed top of the lens was protected by a covering of a silicone adhesive (Kwik-
123 cast - World Precision Instruments). 4 to 8 weeks after GRIN lens implantation, mice were anesthetized
124 and placed in the stereotaxic setup. A baseplate (BPL-2; Inscopix) attached to the miniature microscope
125 was positioned above the GRIN lens. Concentration of the anesthetic gas was lowered and the focal plane
126 was adjusted until neuronal structures and GCaMP6s dynamics were clearly observed. Mice were then
127 fully anaesthetized again and the baseplate was fixed using C&B Metabond (Parkell). A baseplate cap
128 (BCP-2, Inscopix) was left in place until imaging experiments.

129 Behavioral assays

130 Conditioned place preference with food reward

131 The conditioned place preference behavior was motivated by previous work (Stern et al., 2018). It was
132 conducted in a custom-built arena made of two-chambers: a rectangular shaped chamber (45*15 cm) and
133 a triangular shaped chamber (45*30 cm) separated by a corridor (Fig. 1A). Chambers additionally differed
134 based on the texture of the floor and pattern on the walls. The area size of the two chambers were
135 identical. On the first day of the behavioral experiment, mice were allowed to explore the arena for 20
136 min. Preferences for the two chambers were measured and the least preferred one was chosen as the
137 food-paired chamber (context +) for the rest of the paradigm. From then on, and until the end of the
138 experiment, mice were singly housed and food restricted. They were weighed daily and supplied with
139 necessary food to maintain at least 85% of their initial body weight. Conditioning was then conducted
140 over four consecutive days. For this, mice were first sequestered in the neutral context for 15 min and
141 then manually transferred to the positive context for 15 min in which they had access to a food pellet of
142 approximately 1 g. The remaining food was weighed at the end of each conditioning session to determine
143 food consumption. On the 5th and final day of the experiment, mice were allowed to freely navigate
144 between the two chambers in the absence of food. The preference for the positive context was measured
145 for a period of 10 min as a readout for contextual appetitive conditioning. For Ca²⁺ imaging experiments,
146 mice were subjected to the same behavioral task and at the end of the 10 min recall session, we added a
147 food pellet to the positive context and recorded the activity of CeA cells for another 10 min.

148 We had previously performed pilot experiments with WT animals in which 3 groups of 5 mice were
149 conditioned either for 2, 4, or 5 days and the preference of each group for the positive chamber was
150 tested 24hr after the last conditioning day. We found that preference for the appetitive chamber
151 increased from 53.6% +/-1.3 to 71.9% +/-7.6 when we increased the conditioning from 2 to 4 days but did

not increase further when performing the experiment for 5 conditioning days ($PI = 61.7\% \pm 5$) (data not shown). We therefore chose to perform 4 days of conditioning because a preference of 70% for the food-paired chamber would give us a perfect range to identify both increases and decreases in our optogenetic experiment. In our imaging experiment, we also needed animals that would move a lot between the two chambers and spend a sufficient amount of time in both contexts so that we could see both an increase in activity in the positive chamber and a decrease in activity in the neutral one.

For the optogenetic experiments, PKC δ -eNpHR3.0, PKC δ -mCherry, Sst-eNpHR3.0 and Sst-mCherry mice bilaterally received constant 561-nm intracranial light (15 mv) either during the whole 30 min of the conditioning (both in the positive and neutral context) and during all 4 conditioning sessions, or during the whole recall session only. For this, mice were tethered to optic-fiber patch cables (Doric Lenses or Thorlabs) connected to a 561 nm CNI laser (Cobolt) via a rotary joint (Doric Lenses) and mating sleeve (Thorlabs). During habituation and recall, mice were free of the optic-fiber patch cables.

Animals that did not explore both chambers at least once during recall were excluded. This includes 1 PKC δ -eNpHR3.0, 1 PKC δ -mCherry and 1 Sst-eNpHR3.0 animals used for the experiment in Fig. 1G-O and 1 PKC δ -eNpHR3.0, 1 Sst-mCherry and 2 Sst-eNpHR3.0 animals used for the experiment in Fig. 3.

Open-field

PKC δ -eNpHR3.0, PKC δ -mCherry, Sst-eNpHR3.0 and Sst-mCherry mice were allowed to explore a custom-built Plexiglas arena (40 cm \times 40 cm \times 25 cm) for 10 min. During the experiment, mice bilaterally received constant 561-nm intracranial light through optic-fiber patch cords (Doric Lenses or Thorlabs) connected to a 561 nm CNI laser (Cobolt) via a rotary joint (Doric Lenses) and mating sleeve (Thorlabs).

172 Real-time place preference (RTPP)

173 RTPP assays were carried out over two consecutive days. On the first day, PKC δ -eNpHR3.0 and PKC δ -
174 mCherry mice were allowed to explore a custom-built arena made of two chambers (each: 25*25 cm) for
175 20 min. Mice received constant 561-nm intracranial light in one chamber, the photoinhibition-paired
176 chamber. The laser was triggered on the basis of the location of the animal by using Ethovision XT 14
177 software (Noldus). On the next day, the experiment was repeated under the same conditions as on day
178 one, except that the photoinhibition-paired chamber was switched.

179 Conditioned place preference without food reward

180 Conditioned place preference experiments without food reward were carried out in a similar manner as
181 conditioned place preference experiments with food reward except that the inhibition of CeA^{PKC δ} neurons
182 was not paired with delivery of a food reward. Briefly, the experiment was conducted in a custom-built
183 square arena (26.5 x 26.5 cm), divided in the middle by a wall with an opening to form two equally sized
184 triangular compartments which the mice could freely navigate between. Chambers differed based on
185 the texture of the floor. On the first day of the behavioral experiment, PKC δ -eNpHR3.0 and PKC δ -mCherry
186 mice were allowed to freely explore the arena for 20 min. Preferences for the two chambers were
187 measured and the least preferred one was chosen as the photoinhibition-paired chamber for the rest of
188 the paradigm. Conditioning was then conducted over four consecutive days in which mice were
189 sequestered for 15 min in each chamber but received constant 561-nm intracranial light only in the
190 photoinhibition-paired chamber in the absence of food. On the 5th and final day of the experiment, mice
191 were able to freely navigate between the two compartments and the preference for the photoinhibition-
192 paired chamber was measured over a 20 min period.

193 **In vivo Ca^{2+} imaging of freely moving mice**

194 All imaging experiments were conducted on freely behaving mice PKC δ -GCaMP6s and Sst-GCaMP6s mice.
 195 GCaMP6s fluorescence signals were acquired using a miniature integrated fluorescence microscope
 196 system (nVoke - Inscopix). Before each imaging session, the miniscope was secured in the baseplate
 197 holder. Mice were habituated to the miniscope attachment procedure 3 days before behavioral
 198 experiments. The analog gain and LED output power were adjusted such that the best dynamic
 199 fluorescence signals were at the focal plane. Settings were kept constant within subjects and across
 200 imaging sessions. Imaging acquisition and behavior were synchronized using the data acquisition box of
 201 the nVoke Imaging System (Inscopix), triggered by the Ethovision XT 14 software (Noldus) through a TTL
 202 box (Noldus) connected to the USB-IO box from the Ethovision system (Noldus). Compressed images were
 203 obtained at 1200 pixels by 800 pixels and 10 frames per second using the Inscopix acquisition software
 204 (Inscopix). We recorded the activities of CeA neurons during habituation, on day 1 and day 3 of
 205 conditioning, and during recall. To minimize photo-bleaching, we limited the duration of acquisition to 3
 206 times 2 min during habituation, 1 times 2 min during conditioning in the neutral context, and 3 times 2
 207 min during conditioning in the positive context. Each recording bout was evenly spaced in time. On recall
 208 day, Ca^{2+} transients were recorded for the full 20 min of the behavioral experiment.

209 **Histology**

210 Animals that underwent behavioral experiments combined with optogenetic manipulations of CeA cells
 211 were anesthetized with ketamine/xylazine (Medistar and Serumwerk) (100 mg/kg and 16 mg/kg,
 212 respectively) and transcardially perfused with phosphate-buffered saline (PBS), followed by 4%
 213 paraformaldehyde (PFA) (1004005, Merck) (w/v) in PBS. Extracted brains were postfixed at 4 °C in 4% PFA
 214 (w/v) in PBS for 12 h, embedded in 4% agarose (#01280, Biomol) (w/v) in PBS and sliced using a Vibratome
 215 (VT1000S - Leica) into 50 or 100- μm free-floating coronal sections.

216 Mice that underwent calcium imaging experiments were anesthetized with ketamine/xylazine (Medistar
217 and Serumwerk) (100 mg/kg and 16 mg/kg, respectively) and decapitated. The head together with GRIN
218 lens implant and baseplate, were fixed at 4 °C in 4% PFA (w/v) in PBS for a minimum of 4 days before
219 dissection of the brain. Extracted brains were sliced using a Vibratome (VT1000S - Leica) into 100- μ m free-
220 floating coronal sections.

221 **Microscopy**

222 Epifluorescence images were obtained with an upright epifluorescence microscope (Zeiss) with 5 \times /0.15
223 or 10 \times /0.3 objectives (Zeiss). Images were minimally processed with ImageJ software (NIH) to adjust for
224 brightness and contrast for optimal representation of the data. A median filter was used to decrease noise.

225 **Quantification and statistical analyses**

226 Extraction of behavioral data for the conditioned place preference assay with food reward

227 In the conditioned place preference assay, the animal location was recorded at 15Hz using a webcam
228 (Logitech) suspended above the arena and velocity as well as the preference index and number of entries
229 to the positive context and the food zone were automatically analyzed by Ethovision XT 14 software
230 (Noldus).

231 For analysis of the calcium recordings, we could not directly score feeding bouts, since we only used a
232 camera that was suspended above the arena. Therefore, we manually scored the amount of time when
233 the animals were on top of the food and chose a criteria of 2.5s as a minimum time to define a feeding
234 bout.

235 Extraction of behavioral data for the open-field task

236 Animal location was recorded at 15Hz using a webcam (Logitech) suspended above the arena and the
237 number of entries to the center of the arena (20 cm × 20 cm square), cumulative duration in center, as
238 well as velocity were assessed with Ethovision XT 14 software (Noldus).

239 Extraction of behavioral data for the RTPP

240 Animal location was recorded at 15Hz using a webcam (Logitech) suspended above the arena and the
241 location of the animal as well as the velocity were assessed using Ethovision XT 14 (Noldus). Cumulative
242 duration in the photoinhibition-paired chamber was averaged across two sessions.

243 Extraction of behavioral data for the conditioned place preference assay without food reward

244 Animal location was recorded at 15Hz using a webcam (Logitech) suspended above the arena and the
245 preference index for the photoinhibition-paired chamber as well as the velocity were assessed using
246 Ethovision XT 14 (Noldus).

247 Extraction of $\Delta F/F$ and temporal registration with behavioral data

248 For imaging data processing and analysis, all videos recorded from one imaging session were combined
249 into a single image stack using the Inscopix data processing software (version 1.3.0 – Inscopix) and saved
250 as a tiff. Tiff files were then processed using the miniscope 1-photon imaging signal extraction pipeline
251 (MIN1PIPE) (Lu et al., 2018), which returns fully processed ROI components with spatial footprints and
252 temporal calcium traces as outputs. Briefly, the data go through different steps of neural enhancing,
253 hierarchical movement correction, and neural signal extraction that combine a first seeds-cleansing step
254 followed by a simplified spatiotemporal CNMF. Behavioral data were finally temporally aligned to the
255 calcium traces using linear interpolation and unix time stamps as references for both datasets.

256 Longitudinal registration of ROIs

257 ROIs from several recording sessions were longitudinally registered using CellReg Matlab GUI (Sheintuch
258 et al., 2017) (<https://github.com/zivlab/CellReg>). In brief, the roifn output variable from the Min1pipe that
259 contains the processed vectorized ROI footprints for each session was transformed in Matlab using:

260 `roi_use = permute(reshape(roifn, pixh, pixw, n), [3, 1, 2]),` where n is the number of ROIs.

261 Transformed ROIs footprints were then registered using CellReg and the following parameters: alignment
262 type: translations and rotations (max rotation in degrees: 30). A maximal distance of 12 microns was used
263 to compute the probabilistic model. The initial and final cell registrations were performed using spatial
264 correlation models. The resulting cell_to_index_map file was used to identify identical ROIs between
265 different days, calculate the total number of recorded cells per animal, and the number of overlapping
266 neurons during the whole recording session.

267 Regressors and correlation analyses

268 Regressors were built as previously described (Miri et al., 2011). For this, the behavior of each mouse in
269 the positive context, food zone or 'on top of the food' (square-wave data sets) was convolved with a kernel
270 with an exponential decay based on the measured half-decay time for GCaMP6s (~0.150 s) (Chen et al.,
271 2013). The resulting predicted calcium traces were then used to compute Pearson's correlation
272 coefficients with the corresponding calcium traces. To classify neurons as 'neurons encoding appetitive
273 context', 'food responsive cells', or 'unresponsive in positive context', we examined which coefficients
274 rise above or below chance by correlating our fluorescent traces to 1000 random regressors that were
275 constructed after randomly shuffling the real behavioral dataset by bouts of 20s. We required a threshold
276 of 1.96 deviation from the standard error of the random coefficients mean (corresponding to the 95%
277 confidence interval) to assign a cell to a particular functional group.

278 Classification of neurons preferentially active in the positive context

279 To quantify which neurons were preferentially active in the positive context compared to the neutral one
280 during conditioning, $\Delta F/F$ transients were z-scored at each time point using the following formula: $(F(t) -$
281 $F_m)/SD$, where $F(t)$ is the $\Delta F/F$ value at a time t , F_m , and SD are the mean and standard deviation of the
282 baseline calculated from time point when the animals were in the neutral context. An average of the single
283 z-scored time points was then calculated for when the animal was located in the positive context. Neurons
284 were considered to be preferentially active in the positive context when the averaged z-scored value
285 exceeded the 1.96 threshold (corresponding to the 95% confidence interval).

286 Decoding of positive and neutral context locations

287 To decode the location of the mice in the positive or neutral context during recall, we used a logistic
288 regression classifier. For decoder training and testing, we used neuronal Ca^{2+} signals expressed as $\Delta F/F$.
289 For each animal, classifiers were trained on 70% of the data during recall and tested on the remaining
290 30%. We computed the prediction score as the average of correct predictions over a 10-fold cross-
291 validation procedure. Correct predictions were defined as the ratio of $TP / (TP + FP + FN)$ where TP is the
292 number of true positives, FP the number of false positives and FN the number of false negatives.

293 To evaluate the statistical significance of decoding performance, we trained logistic regression decoders
294 on temporally shuffled behavioral data. For this, behavioral data were split into 7 sec bouts and randomly
295 shuffled. This was repeated 5 times. The shuffled prediction score was defined as the average of correct
296 predictions of these 5 repetitions.

297 Alignment of calcium responses to positive and neutral context entries

298 $\Delta F/F$ transients were z-scored with the baseline calculated from time points when the animals were in the
299 neutral context for alignment to positive context entries, or with the baseline calculated from time points

300 when the animals were in the positive context (for alignment to neutral context entries) (see formula
301 above in: Classification of neurons preferentially active in the positive context). We omitted short bouts
302 whose duration was below 2.5 sec to exclude epochs when the animals were only shortly going in and out
303 of the corridor space without fully entering the context. Z-scored calcium responses of single neurons to
304 context entry were then averaged in a time window from 3 s before transition to 4.5 s after. Cells were
305 finally sorted in a descending order based on their activity response upon entry in the + context.

306 Heatmaps of the spatial Ca²⁺ activity

307 To plot a heatmap of the average spatial activity of one selected cell we used the raw $\Delta F/F$ data. The total
308 activity in a specific x-y location was normalized to the total time the animal spent in that location. x-y
309 data were discretized in 50 x 50 pixels.

310 Statistical analysis

311 No statistical methods were used to pre-determine sample sizes. The numbers of samples in each group
312 were based on those used in previously published studies. Behavioral experiments were conducted by an
313 investigator with knowledge of the animal genotype and treatment. For behavioral and *in vivo* imaging
314 experiments, behavioral-tracking software and custom-written Python scripts were used to obtain and
315 analyze the data in an automated and unbiased manner. Statistical analyses were performed with Prism
316 5 (GraphPad) and all statistics are indicated in the figure legends. t-tests were used for individual
317 comparisons of normally distributed data. When normality was not assumed, Mann-Whitney U test and
318 Wilcoxon signed-rank test (for paired observations) were performed for individual comparisons. A one-
319 way repeated measures ANOVA or Friedman's test (as a non-parametric equivalent) was used for within-
320 subject comparisons followed by Bonferroni post hoc analysis or Dunn's multiple comparison test. After
321 the conclusion of experiments, virus-expression, optic-fiber and GRIN-lens placement were verified. Mice

322 with null virus expression as well as mice in which both optical fibers were wrongly located or at least
 323 more than 500 μm above the CeA were excluded from analysis.

324 **Data and code availability**

325 The datasets supporting the current study have not been deposited in a public repository but are available
 326 from the corresponding author on request. This study used custom-built Python 3.0 programmed scripts
 327 that are also available from the corresponding author upon request.

328 **Results**

329 **Inhibition of CeA^{PKC δ} neurons impairs contextual appetitive conditioning**

330 To assess the contributions of CeA subpopulations to the acquisition of contextual appetitive memories,
 331 we trained mice in conditioned place preference experiments to associate one chamber (positive context)
 332 of a two-chamber arena with a food reward (Fig. 1A). Following conditioning, we measured the amount
 333 of time the mice spent in the positive context in the absence of food as a readout for contextual appetitive
 334 learning. Typically, WT mice learned the task well, spending on average 71.9 \pm 7.2 % of their time in the
 335 positive context (Fig. 1B).

336 We focused on CeA^{PKC δ} and CeA^{Sst} neurons, because they represent two non-overlapping populations of
 337 central amygdala cells, representing the majority of all neurons in this region (Kim et al., 2017), and, when
 338 studied in parallel, mediate antagonizing behaviors (Kim et al., 2017; Wilson et al., 2019; Kargl et al., 2020).
 339 We optogenetically inhibited either CeA^{PKC δ} or CeA^{Sst} neurons during all conditioning sessions (in both the
 340 positive and the neutral contexts) by transducing the CeAs of *Prkcd-Cre* or *Sst-Cre* animals with Cre-
 341 dependent halorhodopsin-expressing virus (eNpHR3.0-mCherry) and placing optic fibers bilaterally above
 342 the CeA (Fig. 1C-F). Control mice expressing mCherry behaved similarly to WT mice, although their
 343 preference index (PI) after learning was slightly lower (61.4 \pm 2.9 % for PKC δ mCherry, and 69 \pm 5.1 %

344 for Sst mCherry mice) (Fig. 1G-I). Silencing of CeA^{Sst} neurons did not alter behavior (Fig. 1G-H). In contrast,
 345 CeA^{PKCδ} neuron-inhibited mice showed poor learning performance, lacking a preference for the positive
 346 context during recall (Fig. 1G,I). In addition, CeA^{PKCδ}, but not CeA^{Sst}, neuron-inhibited animals spent
 347 significantly less time in the food zone of the positive context (Fig. 1J-L), even though they visited it with
 348 the same frequency as control mice (Fig. 1M).

349 Several other parameters that may have influenced the outcome of this learning paradigm were found to
 350 be similar between the experimental groups, including velocity during recall (Fig. 1N), the amount of food
 351 eaten during training (Fig. 1O), and the degree of anxiety as measured by duration and entries to the
 352 center, as well as velocity, in an open field task (Fig. 1P-T).

353 We further controlled whether inhibition of CeA^{PKCδ} neuron activity could lead to an assignment of
 354 negative or positive valence to both contexts in the absence of food, which could have interfered with the
 355 contextual appetitive conditioning. In a real time place preference assay (RTPP), we found that CeA^{PKCδ}
 356 neuron-inhibited mice exhibited neither a preference nor an aversion for the photoinhibition-paired
 357 chamber (Fig. 2A-E). We then performed similar conditioned place preference experiments as described
 358 in Fig. 1A but in the absence of a food reward while photoinhibiting CeA^{PKCδ} cells in one chamber over 4
 359 conditioning days. When we tested the preference of the animals for the photoinhibition-paired chamber,
 360 we found that inhibition of CeA^{PKCδ} neurons alone without food, did not produce a conditioned place
 361 preference, nor an aversion for the photoinhibition-paired chamber (Fig. 2A-B and F-I) indicating that
 362 inhibition of these cell's activity alone did not participate in assigning a rewarding or an aversive signal.

363 We next examined the roles of these two populations during memory retrieval or expression. We used
 364 the same tools as before (Fig. 1C) except this time, we selectively inhibited CeA^{PKCδ} or CeA^{Sst} cells only
 365 during the recall phase. Similar to inhibition of CeA neurons during the conditioning phase, we found that
 366 inactivation of CeA^{PKCδ}, but not CeA^{Sst}, cells significantly decreased the preference of the animals for the

positive context compared to control mice (Fig. 3A-F), although the time spent in the food zone (Fig. 3G-I), as well as the frequency of visits (Fig. 3J) remained unchanged. Control parameters such as the velocity during recall (Fig. 3K), and amount of food eaten during training (Fig. 3L) were similar between groups. Overall, these results suggest that CeA^{PKCδ} neurons may play a role in forming and retrieving associations between contextual cues and food availability.

***In vivo* recordings of CeA^{PKCδ} and CeA^{Sst} neuron activity during appetitive conditioning**

To understand how CeA^{PKCδ} and CeA^{Sst} neuron activity differentially contributes to this behavior, we expressed the GCaMP6s indicator in the CeA of PKCδ+ and Sst+ cells and recorded the dynamics of fluorescent signals using a miniscope during all phases of the task (Fig. 4A-C). Mice were subjected to the same behavioral task and at the end of the recall, a food pellet was added to the positive context to make sure that we could functionally tag 'food responsive' neurons.

We recorded the activities of 24–61 cells per mouse, (202 cells total) in 5 Prkcd-cre mice, and 14–60 cells per mouse, (149 cells total) in 5 Sst-cre animals (Fig. 4D). The numbers of active cells during training and recall were higher as compared to habituation day in both groups. Longer imaging time during training and especially recall may account for this difference. Alternatively, investigation and consumption of food may have recruited new sets of neurons (Fig. 4C, D). Using a ROIs alignment method (Sheintuch et al., 2017), we registered cell identities across imaging sessions. We found approximately 10 % of cells in common for all four recording days (Fig. 4E). When excluding the habituation day, the number of common cells increased to about 17% in both Cre lines (Fig. 4E), suggesting that neurons recorded during conditioning and recall may be functionally more similar than the ones initially active during habituation. Of 10 recorded mice, 3 per genotype showed a PI ≥ 50% during recall which is lower than observed before (Fig. 4F). It is possible that the weight of the miniscope rendered movements more laborious and decreased performance. Nonetheless, 8 animals out of 10 increased their preference for the positive

context after conditioning (Fig. 4F), spending on average 2.1 times longer in the food zone and visiting it 1.7 times more often compared to the other 3 corners of the arena (Fig. 4G-H). All together, these are good indications that those 8 animals learned the task.

Central amygdala encoding of Pavlovian appetitive learning

We tested the Hebbian model of appetitive conditioning (D. O. Hebb, 1949; Brown et al., 1990; Sejnowski, 1999) by investigating whether the positive context which represents multisensory information, could serve as a general predictor of food availability after learning. Or, in other words, could CeA neurons that fire during food intake acquire a specific response to the positive context after learning?

Taking into account only the data of the 8 mice that learned the task (Fig. 4F-H), we convolved the positive context signal with the kinetics of the calcium indicator to create a regressor and correlated the activity of each CeA cell with the corresponding regressor across time (Miri et al., 2011). An example trace of a positive context regressor is shown at the bottom of Fig. 5K. We found that during habituation, the activities of all neurons showed little correlation to the positive context. Instead, during recall, the activities of both populations shifted toward positive correlations (Fig. 5A-B), suggesting that the representations of the positive chamber by CeA^{PKC δ} and CeA^{Sst} neurons were transformed after learning.

For each mouse, we randomly selected 70% of the data during recall to train a logistic regression classifier and asked whether, in the remaining dataset, the location of the mice in the positive context, could be accurately predicted based on CeA^{PKC δ} and CeA^{Sst} population activity. In all mice tested, we could reliably decode the position of the animals in the positive chamber ($70.7 \pm 4.7\%$ for CeA^{PKC δ} and $70 \pm 4.1\%$ for CeA^{Sst} recorded ensembles), while performances significantly dropped when the decoder was trained on temporally shuffled behavioral data (Fig. 5C), indicating that correct predictions were well above chance. We also found a decreased performance of 10% and 15%, respectively, when the classifier was tested on CeA^{PKC δ} and CeA^{Sst} population activity that excluded the 4 most important features (defined here as the

neurons showing the highest correlations to the positive context) (Fig. 5C). This suggests that at least a fraction of both populations encoded essential information about the location of the animal in the positive context. When we aligned the neuronal Ca^{2+} responses of each cell to the onset of the transitions from the neutral to the positive context and averaged the data, we found that a subset of both $\text{CeA}^{\text{PKC}\delta}$ and CeA^{Sst} neurons was activated upon transition to the positive context (Fig. 5D-E). During habituation, we could not identify a group of neurons whose activity reliably increased upon entry in the positive chamber, meaning that encoding of the appetitive context by $\text{CeA}^{\text{PKC}\delta}$ and CeA^{Sst} neurons arose after conditioning (Fig. 5D-E). These cells exhibited an area-biased activity that was specifically high when the mouse was in the appetitive context and preferentially within the food corner (Fig. 5F-G). Cells that displayed a significant correlation toward the positive context regressor accounted for about 14.5% of $\text{CeA}^{\text{PKC}\delta}$ and 8.7% of CeA^{Sst} recorded cells during recall (Fig. 5H-I). Neurons encoding appetitive context were found in 4/4 Prkcd -cre analyzed mice and 3/4 analyzed Sst -Cre mice (Fig. 5-1A). Analysis of the $\Delta F/F$ traces revealed different patterns of activity within the positive context. Some neurons fired both upon entry to the positive chamber and investigation of the food zone (Fig. 5J,L, cells 4 and 6, Fig. 5K,M, cell 15). Some cells were active preferentially within the food zone (Fig. 5K,M, cell 11). Other non-memory neurons showed no preference for the positive context nor the food zone (Fig. 5J-M, cells 22 and 23). At this point, no differences were observed between neurons encoding appetitive context within the $\text{PKC}\delta$ and Sst populations. Again, using a regressor-based approach, we found that the activities of 60% of $\text{CeA}^{\text{PKC}\delta}$ and all CeA^{Sst} neurons encoding appetitive context were significantly upregulated during food consumption on the same recall day (Fig. 5N-O and Fig. 5-1A), demonstrating that a subset of these cells can be tagged as food responsive.

We also looked at neurons that would be particularly unresponsive in the positive context (i.e significant negative correlation to the positive context regressor), and identified a total of 9 $\text{PKC}\delta$ + and 7 Sst + neurons. The activity of these neurons was however very weak, as only 6 of them showed a significantly

437 elevated activity in the neutral context (Fig. 5J-M, cells 17 and 21 and Fig. 5-1B). None of these 6 identified
438 neurons nor any other recorded cells showed an increased activity upon transition to the neutral context
439 (Fig. 5P-Q). Additionally, we trained the logistic regression classifier on the presence of the mice in the
440 neutral context while omitting the neurons encoding appetitive context for each animal (Fig. 5H-I). By
441 doing so, we found that performance of the decoder was low ($41.2\% \pm 14.3\%$ for Prkcd-cre, and 48.4%
442 $\pm 19.5\%$ for Sst-cre recorded mice) (Fig. 5R). This is a good indication that there may not be any other
443 neurons (besides the neurons encoding appetitive context), whose activity can be used to predict the
444 location of the animal in the neutral context.

445 We found no correlation between the number of neurons encoding appetitive context and the learning
446 index (data not shown), but this could be an issue inherent to the behavioral task: while the 'poor learners'
447 may associate only the precise location of the food zone with a rewarding outcome, the 'good learners'
448 may associate the whole positive context or even the whole arena with food delivery. In the latter case,
449 neurons encoding appetitive context may already fire when the animal recognizes the whole arena but
450 we do not have the means to visualize them.

451 This hypothesis is supported by the fact that neurons encoding appetitive context, whose activity best
452 represented the food zone, were found in mice that showed lower learning indices, demonstrated as a
453 negative correlation between the average correlation of neurons encoding appetitive context to the food
454 zone regressor and the PI of the mice (Fig. 5S). Additionally, when we compared the prediction scores of
455 our logistic regression decoder with the PI of the mice, we found that decoding accuracy of the classifier
456 decreased with learning performances (Fig. 5T). In other words, the classifier did not manage to find a
457 good representation of the positive context in the neural activity of the 'best learners'. It is therefore
458 possible that mice that learned best generalized the representation of the positive context to the whole
459 arena.

Overall, these results suggest that contextual information associated with the positive context became predictive of food delivery after learning and support a model in which groups of CeA^{PKCδ} and CeA^{Sst} neurons encode contextual food cues in line with a Hebbian plasticity mechanism.

Differences in calcium activity patterns between CeA^{PKCδ} and CeA^{SST} neurons

Next, we took a step back and examined the activity profiles of all recorded neurons during conditioning, taking into consideration all 5 Prkcd-cre and 5 Sst-cre recorded animals (Fig. 4F). On day 1 and day 3 of training, we found that a large fraction of both CeA^{PKCδ} and CeA^{Sst} neurons strongly increased their activity, specifically when the mice were sequestered in the positive context when the food reward was present (Fig. 6A-B and 6C-D, cells A to F). These cells accounted for $30.9 \pm 10.3\%$ of PKCδ and $31.1 \pm 7.3\%$ of Sst recorded ensembles on day 1, and their proportion increased to $41.7 \pm 6.7\%$ and $58.3 \pm 7.8\%$, respectively, on day 3 of conditioning (Fig. 6E).

For each cell, we calculated Pearson's correlations for their corresponding feeding regressor and accordingly classified neurons as activated by food consumption. Interestingly, we observed that CeA^{PKCδ} cells did not always fire systematically during each feeding bout (Fig. 6C). Conversely, CeA^{Sst} neurons increased their activities at the onset of a feeding bout, and more reliably for the next following ones (Fig. 6D). Supporting these observations, on day 1 and on day 3 of training, CeA^{Sst} neurons showed stronger positive correlation to the feeding regressor (Fig. 6F-G) compared to CeA^{PKCδ} cells, and the proportion of food responsive cells was higher among the CeA^{Sst} population (Fig. 6H). There was no difference in the fraction of PKCδ+ and Sst+ cells active in the positive context during training (Fig. 6E), suggesting that the activity of CeA^{PKCδ} cells may not directly relate to food consumption but rather to the salience of the food reward. This phenotype was not because Pkcd-Cre animals ate less than Sst-Cre, as there was no positive correlation between the amount of time spent eating and the proportion of food responsive cells on day 3 of training (Fig. 6I-J).

483 We then tracked neurons over time to see whether they would maintain their food responsiveness over
 484 time and indeed, we found that the majority of cells that showed significant correlation to the feeding
 485 regressor on one conditioning day conserved their functional tag on the subsequent day (Fig. 6C-D, cells
 486 B, D, E and F, and Fig. 6K). Additionally, when tracking PKC δ + and Sst+ cells that were classified as food
 487 responsive on recall, we found that 83% of PKC δ + and Sst+ were also found food responsive on day 3, and
 488 22% of PKC δ + and 50% of Sst+ on day 1 (Fig. 6L-N). In comparison, the majority of non-food responsive
 489 neurons on recall day were classified non-responsive during the whole task (Fig. 6L-N). Most food
 490 responsive neurons were also significantly active in the positive context compared to the neutral one
 491 during all training sessions and were absent during habituation (Fig. 6C, cells B and C, Fig. 6D, cells D to F
 492 and Fig. 6M-O), together revealing their functional selectivity.

493 When tracing back the origin of the PKC δ and Sst neurons encoding appetitive context (Fig. 5-1A) we
 494 identified two different scenarios:

495 1) When detected, cells were tagged as food responsive during each step of the whole paradigm and they
 496 were absent during habituation. This scenario includes 60% of the CeA^{PKC δ} and all CeA^{Sst} neurons encoding
 497 appetitive context.

498 2) Cells were either not food responsive or lost their 'food responsive' tag after conditioning. This includes
 499 40% of the PKC δ neurons encoding appetitive context (found in 2 mice).

500 These last findings suggest that during conditioning, CeA^{Sst} cells whose activities show high positive
 501 correlation with food intake behavior may be important to link environmental information with the
 502 physical properties of the food. In contrast, CeA^{PKC δ} neurons that are robustly activated upon food pellet
 503 delivery in the arena, but not reliably upon food consumption, might rather form associations between
 504 environmental information and the salience of the food reward.

505 Discussion

506 Here, we used a conditioned place preference assay allowing us to identify neuronal correlates of
 507 appetitive memories as the animal freely moves toward the food. This is noticeably different from classical
 508 studies of associative learning that looks at neuronal activity shortly following exposure to a conditioned
 509 tone applied by the experimenter (Pare and Quirk, 2017).

510 We found that two genetically distinct populations of CeA neurons (PKC δ + and Sst+ neurons), developed
 511 specific activity patterns for the chamber associated with the reward. Interestingly, only the activities of
 512 CeA^{PKC δ} , but not CeA^{Sst}, cells were required for the formation and early retrieval of a preference for the
 513 appetitive context, suggesting that these neurons encode a combination of sensory, reward and
 514 contextual information to support learning that a spatial location predicts food availability.

515 CeA^{PKC δ} neurons were previously shown to inhibit appetitive behaviors in response to threats or aversive
 516 tastes, or in response to satiety (Cai et al., 2014; Kim et al., 2017). Moreover, CeA^{PKC δ} neurons could be
 517 described as 'broadly aversive', since these cells also promote pain-related responses, and are linked to
 518 the expression of aversive memories (Haubensak et al., 2010; Cui et al., 2017; Wilson et al., 2019). Our
 519 findings, instead, suggest that CeA^{PKC δ} cells may have functions that are more general and relate to a
 520 variety of stimuli. This is supported by findings from anesthesia neurons which show an 80% overlap with
 521 CeA^{PKC δ} neurons and attenuate (rather than promote) pain-related behavior (Hua et al., 2020). CeA^{Sst}
 522 neurons may also show multidimensional response properties, since these neurons relate to appetitive
 523 stimuli (Kim et al., 2017; Wilson et al., 2019), but also contribute to the generation of defensive behaviors
 524 (Li et al., 2013; Penzo et al., 2015; Yu et al., 2016). Although, these findings underscore the notion that
 525 molecularly distinct populations represent functionally specialized units, it remains possible that further
 526 subdivision of CeA populations using two or three genetic markers will reveal the presence of more
 527 specialized cells.

528 How could CeA^{PKC δ} neurons mediate learning of contextual food cues?

529 Inhibition of CeA^{PKC δ} neurons during conditioning, did not affect the number of times an animal visited the
 530 precise location of the food zone, but rather the time spent within this area. This was consistent with our
 531 calcium imaging data showing that CeA neurons encoding appetitive context showed a significant increase
 532 in activity when the animal was either specifically in the food zone or in the positive context. We interpret
 533 these results such that the activity of CeA neurons may be relevant to encode a representation of the
 534 goal, i.e. reward associated with a particular location, rather than a representation of compass cues that
 535 would help the animal in its search for the food. In the animals that learned best, this memory may initially
 536 be linked to the location of the food zone and was then generalized to the positive context and ultimately
 537 to the whole arena. Inhibition of CeA^{PKC δ} neurons during recall also impaired the preference of the animals
 538 for the positive context, although the effect was weaker and the time spent within the food zone was
 539 unaffected. This suggests that CeA^{PKC δ} cells may be involved in the early retrieval of appetitive memories
 540 but these memories may be gradually transferred to different brain regions over time (Do Monte et al.,
 541 2016).

542 Although contextual memory traces were observed in subsets of both CeA^{PKC δ} and CeA^{Sst} neurons, our
 543 data uncovered differences between their activity patterns. We found for instance, that the proportion
 544 of neurons active during food intake was significantly higher among the CeA^{Sst} compared to the CeA^{PKC δ}
 545 population. We hypothesize that CeA^{Sst} neurons encoding appetitive context may be essential to link a
 546 context or a sensory stimulus with the physical properties of food (e.g. taste, texture, etc), but preventing
 547 this association from forming does not prevent the animals from developing a preference for the food-
 548 paired chamber. Conversely, CeA^{PKC δ} neurons encoding appetitive context may mediate the association
 549 of contextual stimuli with the general affective properties of food, a function that has been previously
 550 suggested for the CeA (Balleine and Killcross, 2006). Inhibiting the formation of these memories would
 551 then impair an animal's ability to develop a preference for the location of the food reward. It is however

important to mention here that our conclusions were drawn based on loss of function experiments of the entire population but with relevant neuronal activity patterns seen in only a subset of cells. Therefore it is possible that specific inhibition of memory neurons as opposed to whole PKC δ + or Sst+ populations could lead to a different phenotype. Our data are nonetheless consistent with recent evidence that initially, before learning, CeA^{PKC δ} neurons are tuned to stimulus salience but after conditioning, they encode valence discrimination to select the appropriate defensive or appetitive responses (Kargl et al., 2020). Furthermore, CeA^{PKC δ} neurons seem to be part of a bottom-up network that is necessary to relay reinforcement signals to higher order areas such as the insula cortex (Kargl et al., 2020) and the lateral amygdala (Yu et al., 2017), which ultimately feed back to the CeA to drive associative learning.

In conclusion, our work reports specific activity patterns of CeA neurons that resemble contextual memory traces to appetitive stimuli. We propose that salience coding in PKC δ + cells is integrated with sensory representations of the environment through Pavlovian learning mechanisms to drive correct behavioral choices during foraging.

Author Contributions

M.P and F.F designed experiments. M.P, F.F and LG performed experiments. M.P analyzed experiments. R.K supervised experiments. M.P and R.K wrote the manuscript. Funding Acquisition, R.K.

References

- Balleine BW, Killcross S (2006) Parallel incentive processing: an integrated view of amygdala function. Trends Neurosci 29:272–279.
- Brown TH, Kairiss EW, Keenan CL (1990) Hebbian Synapses: Biophysical Mechanisms and Algorithms. Annu Rev Neurosci 13:475–511.
- Cai H, Haubensak W, Anthony TE, Anderson DJ (2014) Central amygdala PKC- δ + neurons mediate the

- 574 influence of multiple anorexigenic signals. *Nat Neurosci* 17:1240–1248.
- 575 Chen TW, Wardill TJ, Sun Y, Pulver SR, Renninger SL, Baohan A, Schreiter ER, Kerr RA, Orger MB, Jayaraman
576 V, Looger LL, Svoboda K, Kim DS (2013) Ultrasensitive fluorescent proteins for imaging neuronal
577 activity. *Nature* 499:295–300.
- 578 Ciochi S, Herry C, Grenier F, Wolff SBE, Letzkus JJ, Vlachos I, Ehrlich I, Sprengel R, Deisseroth K, Stadler
579 MB, Müller C, Lüthi A (2010) Encoding of conditioned fear in central amygdala inhibitory circuits.
580 *Nature* 468:277–282.
- 581 Corbit LH, Balleine BW (2005) Double dissociation of basolateral and central amygdala lesions on the
582 general and outcome-specific forms of pavlovian-instrumental transfer. *J Neurosci* 25:962–970.
- 583 Cui Y, Lv G, Jin S, Peng J, Yuan J, He X, Gong H, Xu F, Xu T, Li H (2017) A Central Amygdala-Substantia
584 Innominata Neural Circuitry Encodes Aversive Reinforcement Signals. *Cell Rep* 21:1770–1782
585 Available at: <https://doi.org/10.1016/j.celrep.2017.10.062>.
- 586 D. O. Hebb (1949) *The organization of behavior*. (New York: John Wiley and Sons).
- 587 Do Monte F, Quirk G, Li B, Penzo M (2016) Retrieving fear memories, as time goes by.... *Mol Psychiatry*
588 21:1027–1036.
- 589 Douglass AM, Kucukdereli H, Ponserre M, Markovic M, Gründemann J, Strobel C, Alcala Morales PL,
590 Conzelmann KK, Lüthi A, Klein R (2017) Central amygdala circuits modulate food consumption
591 through a positive-valence mechanism. *Nat Neurosci* 20:1384–1394.
- 592 Ehrlich I, Humeau Y, Grenier F, Ciochi S, Herry C, Lüthi A (2009) Amygdala Inhibitory Circuits and the
593 Control of Fear Memory. *Neuron* 62:757–771.
- 594 Fadok JP, Markovic M, Tovote P, Lüthi A (2018) New perspectives on central amygdala function. *Curr Opin*

- 595 Neurobiol 49:141–147.
- 596 Gallagher M, Graham PW, Holland PC, Graham WP, Holland PC, Graham PW (1990) The amygdala central
 597 nucleus and appetitive Pavlovian conditioning: Lesions impair one class of conditioned behavior. J
 598 Comp Physiol 10:1906–1911.
- 599 Han JS, Holland PC, Gallagher M (1999) Disconnection of the amygdala central nucleus and substantia
 600 innominata/nucleus basalis disrupts increments in conditioned stimulus processing in rats. Behav
 601 Neurosci 113:143–151.
- 602 Han JS, McMahan RW, Holland P, Gallagher M (1997) The role of an amygdalo-nigrostriatal pathway in
 603 associative learning. J Neurosci 17:3913–3919.
- 604 Haubensak W, Kunwar PS, Cai H, Cioocchi S, Wall NR, Ponnusamy R, Biag J, Dong HW, Deisseroth K, Callaway
 605 EM, Fanselow MS, Lüthi A, Anderson DJ (2010) Genetic dissection of an amygdala microcircuit that
 606 gates conditioned fear. Nature 468:270–276.
- 607 Herry C, Johansen JP (2014) Encoding of fear learning and memory in distributed neuronal circuits. Nat
 608 Neurosci 17:1644–1654 Available at: <http://www.nature.com/doi/10.1038/nn.3869>.
- 609 Hua T, Chen B, Lu D, Sakurai K, Zhao S, Han BX, Kim J, Yin L, Chen Y, Lu J, Wang F (2020) General anesthetics
 610 activate a potent central pain-suppression circuit in the amygdala. Nat Neurosci 23:854–868.
- 611 Janak PH, Tye KM (2015) From circuits to behaviour in the amygdala. Nature 517:284–292 Available at:
 612 <http://www.nature.com/doi/10.1038/nature14188> [Accessed January 14, 2015].
- 613 Kargl D, Kaczanowska J, Ulonska S, Groessl F, Piszczek L, Lazovic J, Buehler K, Haubensak W (2020) The
 614 amygdala instructs insular feedback for affective learning. Elife 9:1–36.
- 615 Kim J, Zhang X, Muralidhar S, LeBlanc SA, Tonegawa S (2017) Basolateral to Central Amygdala Neural

- 616 Circuits for Appetitive Behaviors. *Neuron* 93:1464–1479.
- 617 Lee HJ, Groshek F, Petrovich GD, Cantalini JP, Gallagher M, Holland PC (2005) Role of amygdalo-nigral
618 circuitry in conditioning of a visual stimulus paired with food. *J Neurosci* 25:3881–3888.
- 619 Li H, Penzo MA, Taniguchi H, Kopec CD, Huang ZJ, Li B (2013) Experience-dependent modification of a
620 central amygdala fear circuit. *Nat Neurosci* 16:332–339.
- 621 Lu J, Li C, Singh-Alvarado J, Zhou ZC, Fröhlich F, Mooney R, Wang F (2018) MIN1PIPE: A Miniscope 1-
622 Photon-Based Calcium Imaging Signal Extraction Pipeline. *Cell Rep* 23:3673–3684.
- 623 McDannald M, Kerfoot E, Gallagher M, Holland PC (2004) Amygdala central nucleus function is necessary
624 for learning but not expression of conditioned visual orienting. *Eur J Neurosci* 20:240–248.
- 625 Miri A, Daie K, Burdine RD, Aksay E, Tank DW (2011) Regression-based identification of behavior-encoding
626 neurons during large-scale optical imaging of neural activity at cellular resolution. *J Neurophysiol*
627 105:964–980.
- 628 Ozawa T, Ycu EA, Kumar A, Yeh LF, Ahmed T, Koivumaa J, Johansen JP (2017) A feedback neural circuit for
629 calibrating aversive memory strength. *Nat Neurosci* 20:90–97 Available at:
630 <http://www.nature.com/doi/10.1038/nn.4439>.
- 631 Pare D, Duvarci S (2012) Amygdala microcircuits mediating fear expression and extinction. *Curr Opin*
632 *Neurobiol* 22:717–723 Available at: <http://www.ncbi.nlm.nih.gov/pubmed/22424846> [Accessed
633 March 5, 2013].
- 634 Pare D, Quirk GJ (2017) When scientific paradigms lead to tunnel vision: lessons from the study of fear.
635 *npj Sci Learn* 2:1–8.
- 636 Penzo MA, Robert V, Tucciarone J, De Bundel D, Wang M, Van Aelst L, Darvas M, Parada LF, Palmiter RD,

- 637 He M, Huang ZJ, Li B (2015) The paraventricular thalamus controls a central amygdala fear circuit.
638 Nature 519:455–459.
- 639 Sejnowski TJ (1999) The book of Hebb. Neuron 24:773–776.
- 640 Sheintuch L, Rubin A, Brande-Eilat N, Geva N, Sadeh N, Pinchasof O, Ziv Y (2017) Tracking the Same
641 Neurons across Multiple Days in Ca²⁺ Imaging Data. Cell Rep 21:1102–1115.
- 642 Soriano P (1999) Generalized lacZ expression with the ROSA26 Cre reporter strain. Nat Genet 21:70–71.
- 643 Stern SA, Doerig KR, Azevedo EP, Stoffel E, Friedman JM (2018) Control of non-homeostatic feeding in
644 sated mice using associative learning of contextual food cues. Mol Psychiatry:1–14.
- 645 Wilensky AE, Schafe GE, Kristensen MP, Ledoux JE (2006) Rethinking the Fear Circuit : The Central Nucleus
646 of the Amygdala Is Required for the Acquisition , Consolidation , and Expression of Pavlovian Fear
647 Conditioning. 26:12387–12396.
- 648 Wilson TD, Valdivia S, Khan A, Ahn HS, Adke AP, Gonzalez SM, Sugimura YK, Carrasquillo Y (2019) Dual and
649 Opposing Functions of the Central Amygdala in the Modulation of Pain. Cell Rep 29:332-346.e5.
- 650 Yu K, Ahrens S, Zhang X, Schiff H, Ramakrishnan C, Fenno L, Deisseroth K, Zhao F, Luo MH, Gong L, He M,
651 Zhou P, Paninski L, Li B (2017) The central amygdala controls learning in the lateral amygdala. Nat
652 Neurosci 20:1680–1685.
- 653 Yu K, da Silva PG, Albeanu DF, Li B (2016) Central amygdala somatostatin neurons gate passive and active
654 defensive behaviors. J Neurosci 36:6488–6496.
- 655

656 Figures and Legends

657 **Figure 1.** Inhibition of CeA^{PKCδ} neurons during conditioning impairs contextual appetitive conditioning
 658 **A**, Place preference behavioral paradigm. **B**, Preference index (PI) for the positive context+ context before
 659 and after conditioning for WT animals (n = 5 mice). **C**, Optogenetic inhibition of CeA neurons. The CeA of
 660 Prkcd-Cre or Sst-Cre mice was transduced with a Cre-dependent AAV expressing eNpHR3.0-mCherry or
 661 mCherry alone. CeA neurons were photoinhibited *in vivo* with constant yellow light. **D-E**, Representative
 662 epifluorescent images of Prkcd-Cre (D) and Sst-Cre mice (E) injected in the CeL with an AAV-DIO-
 663 eNpHR3.0-mCherry (D₁ and E₁) or AAV-DIO-mCherry (D₂ and E₂) and showing the location of the optic fiber
 664 tract (in yellow). Scale bars: 100 μm. **F** Approximate optic fiber locations for each animal and expression
 665 spread. Locations are shown on schematic coronal section planes with distances (anterior-posterior axis)
 666 from bregma. **G**, PI for the food-paired chamber (+ context) during recall after inhibition of CeA neurons
 667 during conditioning (Mann-Whitney U test, for PKCδ group comparison: U = 1, P = 0.0021 and for Sst group
 668 comparison: U = 29, P = 0.7927). **H-I**, PI for the food-paired chamber before and after conditioning for
 669 CeA^{Sst} (H) and CeA^{PKCδ} neuron-inhibited animals (I), and respective control mice. **J-K**, Representative heat
 670 maps of the behavior of individual PKCδ-eNpHR3.0 and PKCδ-mCherry mice during recall. Green
 671 represents the minimum and purple the maximum per-pixel frequency. **L**, Number of visits to the food
 672 zone during recall (two-tailed unpaired t-test, for PKCδ group comparison: t(13) = 0.5618, P = 0.5838 and
 673 for Sst group comparison: t(14) = 1.772, P = 0.0982). **M**, PI for the food zone during recall (Mann-Whitney
 674 U test, for PKCδ group comparison: U = 10.5, P = 0.0489 and for Sst group comparison: U = 14, P = 0.0650).
 675 **N**, Velocity during recall (two-tailed unpaired t-test, for PKCδ group comparison: t(13) = 0.6142, P = 0.5497
 676 and for Sst group comparison: t(14) = 0.7520, P = 0.4645). **O**, Cumulative amount of food eaten during the
 677 four training days (two-tailed unpaired t-test, for PKCδ group comparison: t(13) = 0.3398, P = 0.7394 and
 678 for Sst group comparison: t(14) = 1.141, P = 0.2730). **P-Q**, Representative traces (in red) of the behavior
 679 of PKCδ-eNpHR3.0 (P₁), PKCδ-mCherry (P₂), Sst-eNpHR3.0 (Q₁) and Sst-mCherry mice (Q₂) during the

openfield task. The yellow square represents the center. **R**, Cumulative duration in center during the openfield task (Mann-Whitney U test, for PKC δ group comparison: $U = 33$, $P = 0.8096$ and for Sst group comparison: $U = 25.5$, $P = 0.8168$). **S**, Number of visits to the center during the openfield task (two-tailed unpaired t-test, for PKC δ group comparison: $t(15) = 1.033$, $P = 0.3181$ and for Sst group comparison: $t(13) = 0.3481$, $P = 0.7334$). **T**, Velocity during the openfield task (two-tailed unpaired t-test, for PKC δ group comparison: $t(15) = 0.6166$, $P = 0.5467$ and for Sst group comparison: $t(13) = 1.348$, $P = 0.2006$). (For panels G-O, $n = 8$ PKC δ -eNpHR3.0 and 7 PKC δ -mCherry mice and $n = 8$ Sst-eNpHR3.0 and $n = 8$ Sst-mCherry mice and for panels P-T, $n = 9$ PKC δ -eNpHR3.0 and 8 PKC δ mCherry mice and $n = 7$ Sst-eNpHR3.0 and $n = 8$ Sst-mCherry mice). Bar graphs show mean \pm s.e.m, each dot is the quantification of a single animal; ns, not significant, $*P < 0.05$, $**P < 0.01$. CeC/L: central capsular and central lateral amygdala; BLA: basolateral amygdala; CeM: central medial amygdala.

691

692 **Figure 2.** Inhibition of CeA^{PKC δ} neurons does not result in assigning a rewarding or an aversive signal.

693 **A**, Representative epifluorescent images of Prkcd-Cre mice injected in the CeL with an AAV-DIO-
 694 eNPHR3.0-mCherry (A₁) or AAV-DIO-mCherry (A₂) and showing the location of the optic fiber tract (in
 695 yellow). Scale bars: 100 μ m. **B**, Approximate optic fiber locations for each animal and expression spread.
 696 Locations are shown on schematic coronal section planes with distances (anterior-posterior axis) from
 697 bregma. **C**, Representative traces of the behavior of PKC δ -eNpHR3.0 (C₁) and PKC δ -mCherry (C₂) during
 698 the RTPP task. **D**, Cumulative duration in the photoinhibition-paired side during the RTPP assay (Mann-
 699 Whitney U test, U = 6.0, P = 0.2222). **E**, Velocity during RTPP (two-tailed unpaired t-test: t(9) = 0.1112, P =
 700 0.9139). **F**, Representative traces of the behavior of PKC δ -eNpHR3.0 (F₁) and PKC δ -mCherry (F₂) during
 701 the CPP without food task. **G**, PI for the photoinhibition-paired chamber during recall after inhibition of
 702 CeA neurons during conditioning and in the absence of food (Mann-Whitney U test: U = 11, P = 0.5368).
 703 **H**, PI for the photoinhibition-paired chamber before and after conditioning for CeA^{PKC δ} neuron-inhibited
 704 animals and respective control mice. (n = 5 PKC δ -eNpHR3.0 and 6 PKC δ -mCherry). **E**, Velocity during CPP
 705 without food (two-tailed unpaired t-test: t(9) = 1.350, P = 0.2099). Bar graphs show mean \pm s.e.m and
 706 each dot is the quantification of a single animal; ns, not significant. CeC/L: central capsular and central
 707 lateral amygdala; BLA: basolateral amygdala; CeM: central medial amygdala.

708 **Figure 3.** Inhibition of CeA^{PKCδ} neurons during recall impairs contextual appetitive conditioning
709 **A-B**, Representative epifluorescent images of Prkcd-Cre (A) and Sst-Cre mice (B) injected in the CeL with
710 an AAV-DIO-eNPHR3.0-mCherry (A₁ and B₁) or AAV-DIO-mCherry (A₂ and B₂) and showing the location of
711 the optic fiber tract (in yellow). Scale bars: 100 μm. **C** Approximate optic fiber locations for each animal
712 and expression spread. Locations are shown on schematic coronal section planes with distances (anterior-
713 posterior axis) from bregma. **D**, PI for the food-paired chamber (+ context) during recall while inhibiting
714 CeA neurons during recall only (Mann-Whitney U test, for PKCδ group comparison: U = 19.5, P = 0.0250
715 and for Sst group comparison: U = 49, P = 0.7491). **E-F**, PI for the + context before and after conditioning
716 for CeA^{Sst} (E), CeA^{PKCδ} neuron-inhibited animals (F), and respective control mice. **G-H**, Representative heat
717 maps of the behavior of individual PKCδ-eNpHR3.0 and PKCδ-mCherry mice during recall. Green
718 represents the minimum and purple the maximum per-pixel frequency. **I**, PI for the food zone during recall
719 (Mann-Whitney U test, for PKCδ group comparison: U = 40.0, P = 0.4941 and for Sst group comparison: U
720 = 27, P = 0.0597). **J**, Number of visits to the food zone during recall (two-tailed unpaired t-test, for PKCδ
721 group comparison: t(18) = 0.2447, P = 0.8094 and for Sst group comparison: t(20) = 0.3566, P = 0.7251).
722 **K**, Velocity during recall (two-tailed unpaired t-test, for PKCδ group comparison: t(18) = 0.8922, P = 0.3840
723 and for Sst group comparison: t(19) = 1.707, P = 0.1041). **L**, Cumulative amount of food eaten during the
724 four training days (two-tailed unpaired t-test, for PKCδ group comparison: t(18) = 0.7204, P = 0.4806 and
725 for Sst group comparison: t(14) = 0.7520, P = 0.0686). (n = 11 PKCδ-eNpHR3.0 and 9 PKCδ-mCherry mice
726 and n = 12 Sst-eNpHR3.0 and n = 9 Sst-mCherry mice). Bar graphs show mean +/- s.e.m, each dot is the
727 quantification of a single animal; ns, not significant, *P < 0.05. CeC/L: central capsular and central lateral
728 amygdala; BLA: basolateral amygdala; CeM: central medial amygdala.

729

730 **Figure 4.** *In vivo* calcium imaging of CeA^{PKCδ} and CeA^{SST} neurons

731 **A**, Calcium imaging of CeA^{PKCδ} and CeA^{Sst} neurons via miniscope in freely moving mice. **B**, Representative
 732 epifluorescent images of Prkcd-Cre (B₁) and Sst-Cre mice (B₂) injected in the CeL with an AAV-DIO-
 733 GCaMP6s-eYFP and showing the location of the GRIN lens tract (in yellow). Scale bars: 100 μm. **C**,
 734 Maximum-projection images of PKCδ+ GCaMP6s-expressing neurons from a representative mouse
 735 recorded during habituation (C₁), first (C₂) and third (C₃) days of training, as well as recall (C₄).
 736 Corresponding region-of-interests (ROIs) are depicted below each panel. ROIs identified over consecutive
 737 sessions are shown in identical color. ROIs detected only in one session are shown in white. Blue
 738 arrowheads indicate neurons that appeared for the first time on day 1 of conditioning. Yellow arrowheads
 739 indicate neurons that are common between at least 2 out of 3 days of conditioning and recall and are not
 740 visible on habituation. **D**, Numbers of detected ROIs during all four sessions (One-way repeated measures
 741 ANOVA, for PKCδ group comparisons: time point, $F(3,4) = 2.16$, $P = 0.1458$ and for Sst group comparisons:
 742 time point, $F(3,4) = 3.98$, $P = 0.0351$). **E**, Percentage of ROIs per Prkcd-Cre and Sst-Cre mouse that
 743 overlapped in all four recording sessions or from day 1 of conditioning to recall (Wilcoxon signed-rank
 744 test, for PKCδ comparison: $P = 0.125$, and for Sst group comparison: $P = 0.25$). **F**, PI for the + context before
 745 and after conditioning for both PKCδ- and Sst-GCaMP6s recorded mice. Data points shown as crossed
 746 circles represent mice that did not show an increase in learning after conditioning. **G**, Cumulative duration
 747 in food zone compared to the averaged cumulative duration in the other three corners for the 4 PKCδ-
 748 and 4 Sst-GCaMP6s mice that are considered to have learned the task (see Fig. 4F). Similar symbols
 749 represent the same mice. **H**, Frequency of visits to the food zone compared to the averaged frequency of
 750 visits in the other three corners for the 4 PKCδ- and 4 Sst-GCaMP6s recorded mice that are considered to
 751 have learned the task (see Fig. 4F). Similar symbols represent the same mice. ($n = 5$ PKCδ-GCaMP6s and n
 752 $= 5$ Sst-GCaMP6s recorded animals). Bar graphs show mean \pm s.e.m, each dot is the quantification of a
 753 single animal. ns, not significant.

754 **Figure 5.** Central amygdala encoding of Pavlovian appetitive learning

755 **A-B**, Frequency distribution of Pearson's correlation to the positive context regressor in PKC δ (A) and SST

756 (B) calcium recorded neurons during habituation and recall. **C**, Prediction scores of the locations of Prkcd-

757 Cre (purple) and Sst-Cre (yellow) calcium recorded animals in the positive context during recall, after

758 temporally shuffling of behavioral data (shuffled) and after excluding 4 neurons per animal that exhibited

759 the highest correlation value to the positive context regressor (recall -) (Friedman test, for PKC δ group

760 comparisons: $F=9.9$, $P=0.0062$ with Dunn's Multiple Comparison Test and for Sst group comparisons: $F =$

761 9.3 , $P = 0.0115$ with Dunn's Multiple Comparison Test, $*P < 0.05$). **D-E**, Heatmaps of average z-scored

762 calcium responses of PKC δ (D) and SST (E) recorded neurons following entry to the positive context (at 0

763 sec) during recall (D_1 and E_1) and during habituation (D_2 and E_2). Cells were sorted in descending order

764 based on their activity response upon entry in the + context (entries to the + context varied from 6 to 14

765 times depending on the mice) ($n = 75$ PKC δ + and 50 Sst+ neurons). **F-G**, Heatmaps of the $\Delta F/F$ signal across

766 the whole arena for one representative PKC δ (F) and Sst (G) neuron encoding appetitive context. Green

767 represents the minimum and purple the maximum per-pixel frequency (see also Fig. 5-1A). **H-I**, Fraction

768 of CeA neurons encoding appetitive context in Prkcd-cre (H) and Sst-cre (I) recorded animals during recall.

769 **J-K**, Representative Ca^{2+} traces (from 7 mice) of PKC δ (J) and Sst (K) recorded neurons during recall. The

770 trace in beige at the bottom of K represents the convolved GCaMP6s regressor for the positive context of

771 cell 21 (see also Fig. 5-1A). Values indicate the Pearson's coefficients of each cell to its corresponding

772 positive context regressor. Values in green indicate a significant negative correlation. Each $\Delta F/F$ trace was

773 normalized to its maximum value. **L-M**, Average traces of the corresponding PKC δ (L) and Sst (M) neurons

774 shown on the left following entry to the positive context (at 0 sec). Cells 4, 6, 15 and 11 are 4

775 representative neurons encoding the appetitive context after learning. Cells 22 and 23 are non-memory

776 cells, cells 17 and 21 are neurons whose activity is negatively correlated to the positive context. Shaded

777 areas represent s.e.m. **N-O**, Ca^{2+} signals of the corresponding PKC δ (N) and Sst (O) neurons shown in

778 figure J-K upon introduction of a food pellet in the food zone (dotted line) at the end of the place
779 preference assay. Values indicate the Pearson's coefficients of each cell to its corresponding feeding bouts
780 regressor. Values in red indicate a significant correlation. Each $\Delta F/F$ trace was normalized to its maximum
781 value. **P-Q**, Heatmap of averaged z-scored calcium responses of PKC δ (P) and SST (Q) recorded neurons
782 following entry to the neutral context (- context at 0 sec). $\Delta F/F$ transients were z-scored with the baseline
783 calculated from time points when the animals were in the positive context. Cells were sorted in
784 descending order based on their activity response upon entry in the - context (n = 75 PKC δ + and 50 Sst+
785 neurons). **R**, Prediction scores of the locations of Prkcd-Cre (purple) and Sst-Cre (yellow) calcium recorded
786 animals in the neutral context during recall. **S**, Preference index (PI) in the positive context on recall day
787 as a function of the averaged value of all Pearson's correlation coefficients to the food zone regressor for
788 all identified neurons encoding appetitive context in a given mouse. Each dot represents a single Prkcd-
789 Cre (purple) or Sst-Cre (yellow) animal. Values shown are R^2 . **T**, Prediction score of the logistic regression
790 classifier as a function of the PI of the animal on recall day. Each dot represents a single Prkcd-Cre (purple)
791 or Sst-Cre (yellow) animal. Values shown are R^2 . (n = 4 PKC δ - and 4 Sst-GCaMP6s recorded animals). Bar
792 graphs show mean \pm s.e.m and each dot represents a single animal. ns, not significant, *P < 0.05.

793

794 **Figure 6.** Differences in calcium activity patterns between CeA^{PKCδ} and CeA^{SST} neurons
 795 **A-B,** Maximum-projection representative images of PKCδ+ (A) and Sst+ (B) GCaMP6s-expressing neurons
 796 during day 3 of conditioning in the neutral (A₁ and B₁) and in the positive context (A₂ and B₂). **C-D,**
 797 Representative Ca²⁺ traces (from 6 mice) of PKCδ (C) and Sst (D) recorded neurons during habituation, day
 798 1, day 3 of conditioning, and recall with food. Colored boxes indicate the location of the mouse in the
 799 corridor (grey) or on top of the food (green). The values indicate the Pearson's coefficients of each cell to
 800 its corresponding feeding bouts regressor. Values in red indicate a significant correlation. Each ΔF/F trace
 801 was normalized to its maximum value. **E,** Proportion of neurons per mouse that are significantly active in
 802 + context compared to - context on days 1 and 3 of conditioning. (Mann-Whitney U test between PKCδ
 803 and Sst on day1, U = 11, P = 0.8413 and on day3, U = 6, P = 0.2045). **F-G,** Frequency distribution of Pearson's
 804 correlations to the feeding bouts regressor in all PKCδ and SST recorded neurons during day 1 (F) and day
 805 3 (G) of conditioning. **H,** Proportion of neurons per mouse that are food responsive on day 1, day 3 of
 806 conditioning, and recall. (Mann-Whitney U test between PKCδ and Sst on day1, U = 10, P = 0.6723, on
 807 day3, U = 2, P = 0.0362 and on recall, U = 4, P = 0.0952). **I,** Time spent eating during day 3 for PKCδ- and
 808 Sst-GCaMP6s recorded mice (two-tailed unpaired t-test t(8) = 2.242, P = 0.552). **J,** Proportion of food
 809 responsive PKCδ+ and SST+ cells as a function of the time spent eating on day 3 of conditioning. **K,**
 810 Heatmaps of Pearson's correlations to the feeding bouts regressor for PKCδ (K₁) and SST (K₂) neurons that
 811 were classified as food responsive on at least one of the recorded days. White represents neurons that
 812 were not detected during a recording session. Blue represents no significant correlations, so non-food
 813 responsive cells. Strong correlation values are represented in dark red. Arrows indicate neurons that were
 814 classified as food responsive on one day and lost their functional tag on the following one. (n = 40 PKCδ+
 815 and 39 SST+ neurons). **L,** Fraction of food responsive (solid lines) and non-food responsive cells (dotted
 816 lines) detected during recall that are tagged as food responsive on day 3 and 1 of conditioning and present
 817 during habituation. **M-N,** Food responsive PKCδ+ (purple lines, M) and Sst+ cells (yellow lines, N) as well

818 as non-food responsive cells (gray lines) detected during recall and traced back to day 3 and day 1 of
819 conditioning and habituation. Each line represents a cell and its correlation value to the feeding regressor
820 on recall, day 3 and day 1 of conditioning, as well as whether it was present or not during habituation.
821 Values above 0.25 represent a significant positive correlation to the feeding regressor ($n = 92$ PKC δ + and
822 59 SST+ neurons). **O**, Proportion of food responsive PKC δ + and SST+ neurons that were active during
823 habituation and that were significantly active in the - context or the + context during day 1 and day 3 of
824 conditioning ($n = 40$ PKC δ + and 39 SST+ neurons). ($n = 5$ PKC δ - and 5 Sst-GCaMP6s recorded animals). Bar
825 graphs show mean \pm s.e.m, each dot represents a single animal. ns, not significant, * $P < 0.05$.

826

827 **Extended data and legends**

828 **Figure 5-1.**

829 **A**, Ca^{2+} traces of all PKC δ and Sst identified neurons encoding appetitive context during each step of the
830 conditioning paradigm (A_1). Values during recall indicate the Pearson's coefficients of each cell to its
831 corresponding positive context regressor. Values during day 1, day 3, and recall with food indicate the
832 Pearson's coefficients of each cell to its corresponding feeding bouts regressor. Values in red indicate a
833 significant correlation. Each $\Delta F/F$ trace was normalized to its maximum value. **A₂**, Heatmaps of the $\Delta F/F$
834 signal across the whole arena. Green represents the minimum and purple the maximum per-pixel
835 frequency. **B**, Ca^{2+} traces of the 6 identified PKC δ and Sst cells that show both a significant negative
836 correlation to the positive context regressor and a significant positive correlation to the neutral context
837 regressor (B_1). Values during recall indicate the Pearson's coefficients of each cell to its corresponding
838 positive context regressor. Values in green indicate a significant negative correlation. Values during day
839 1, day 3, and recall with food indicate the Pearson's coefficients of each cell to its corresponding feeding
840 bouts regressor. Values in red indicate a significant positive correlation. Each $\Delta F/F$ trace was normalized
841 to its maximum value. **B₂**, Heatmaps of the $\Delta F/F$ signal across the whole arena. Green represents the
842 minimum and purple the maximum per-pixel frequency.

Figure 1

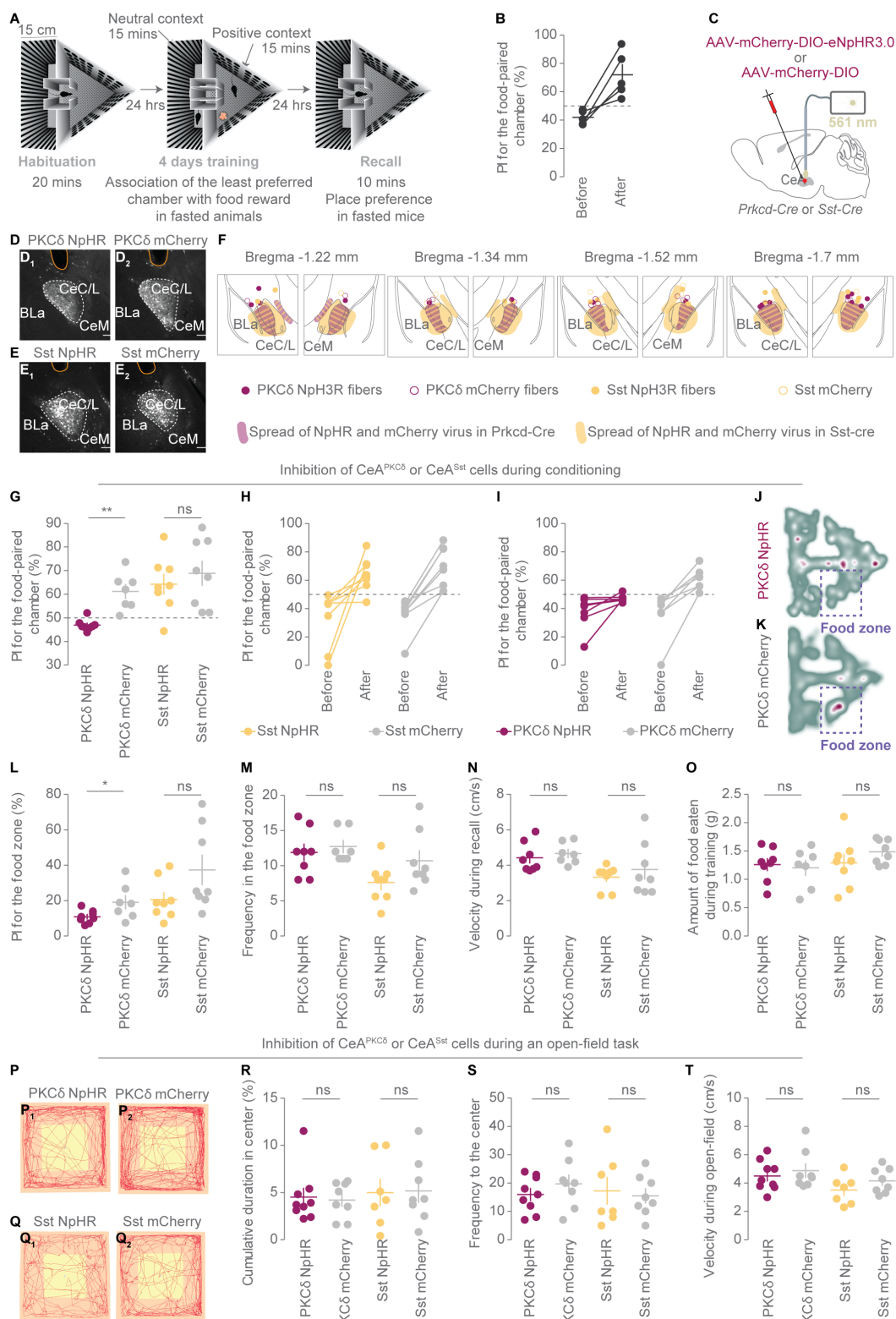


Figure 2

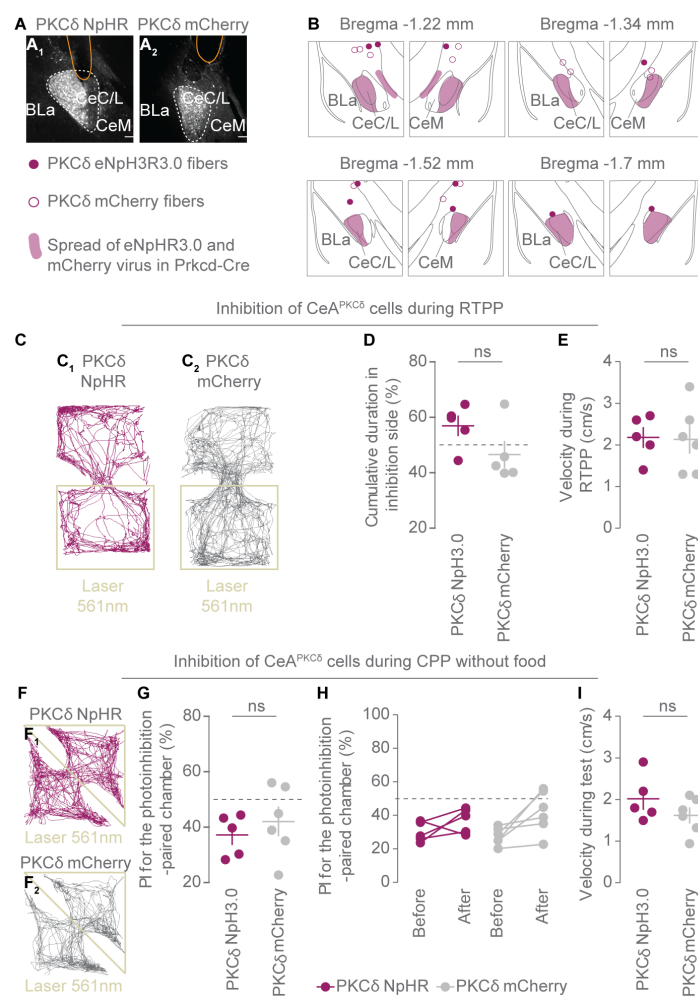


Figure 3

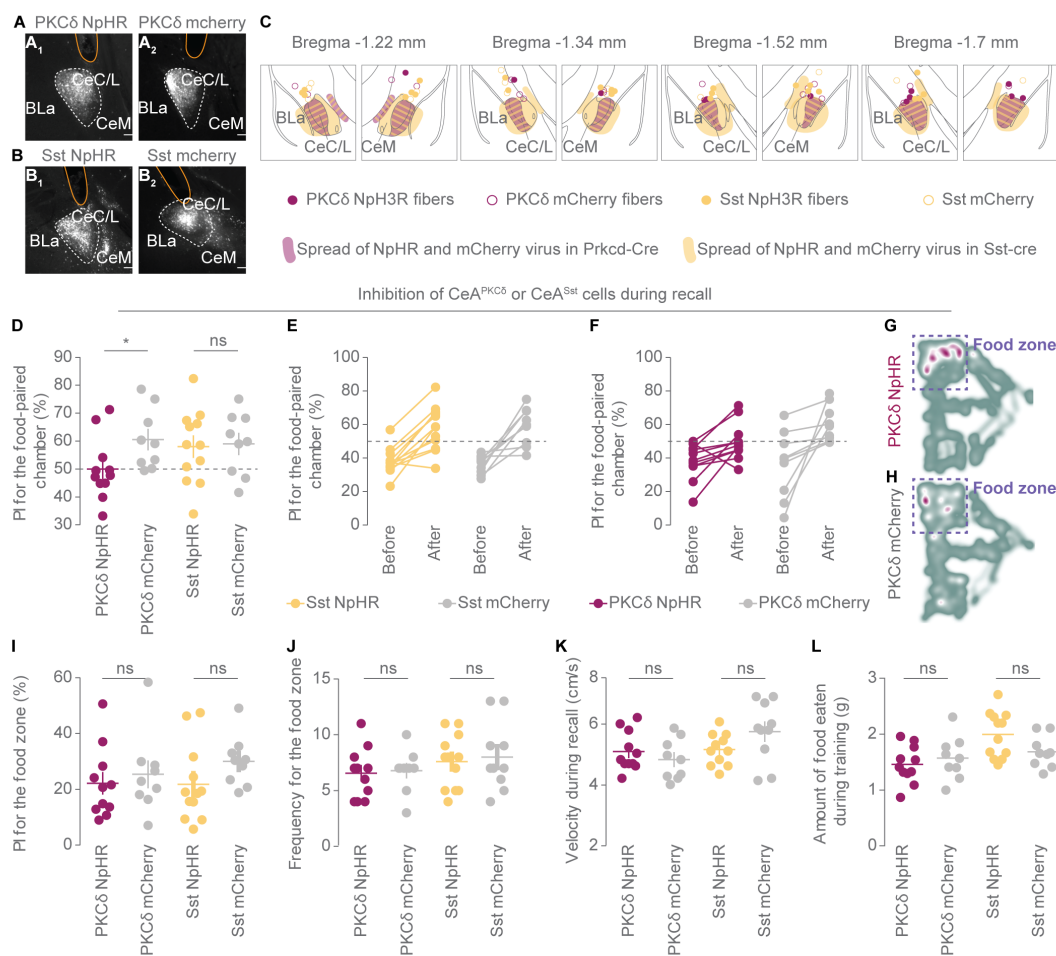


Figure 4

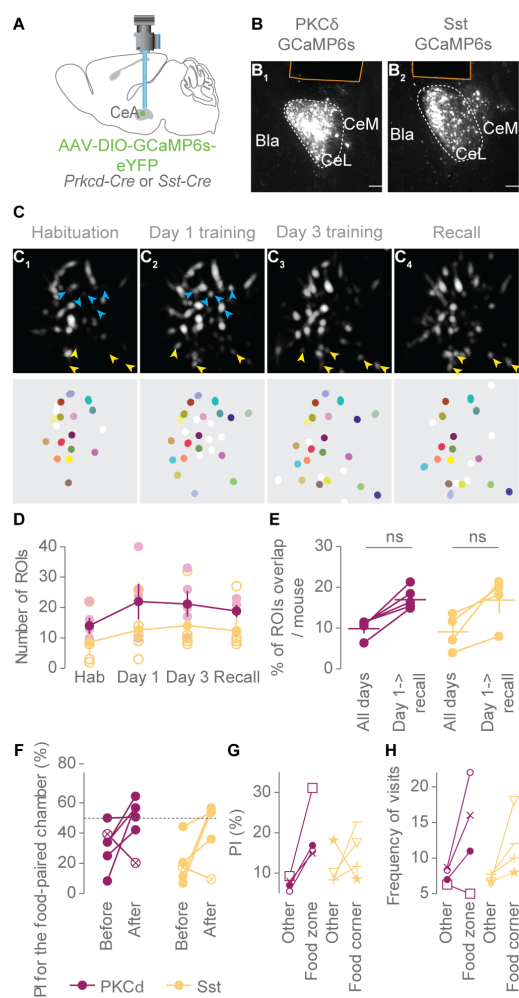


Figure 5

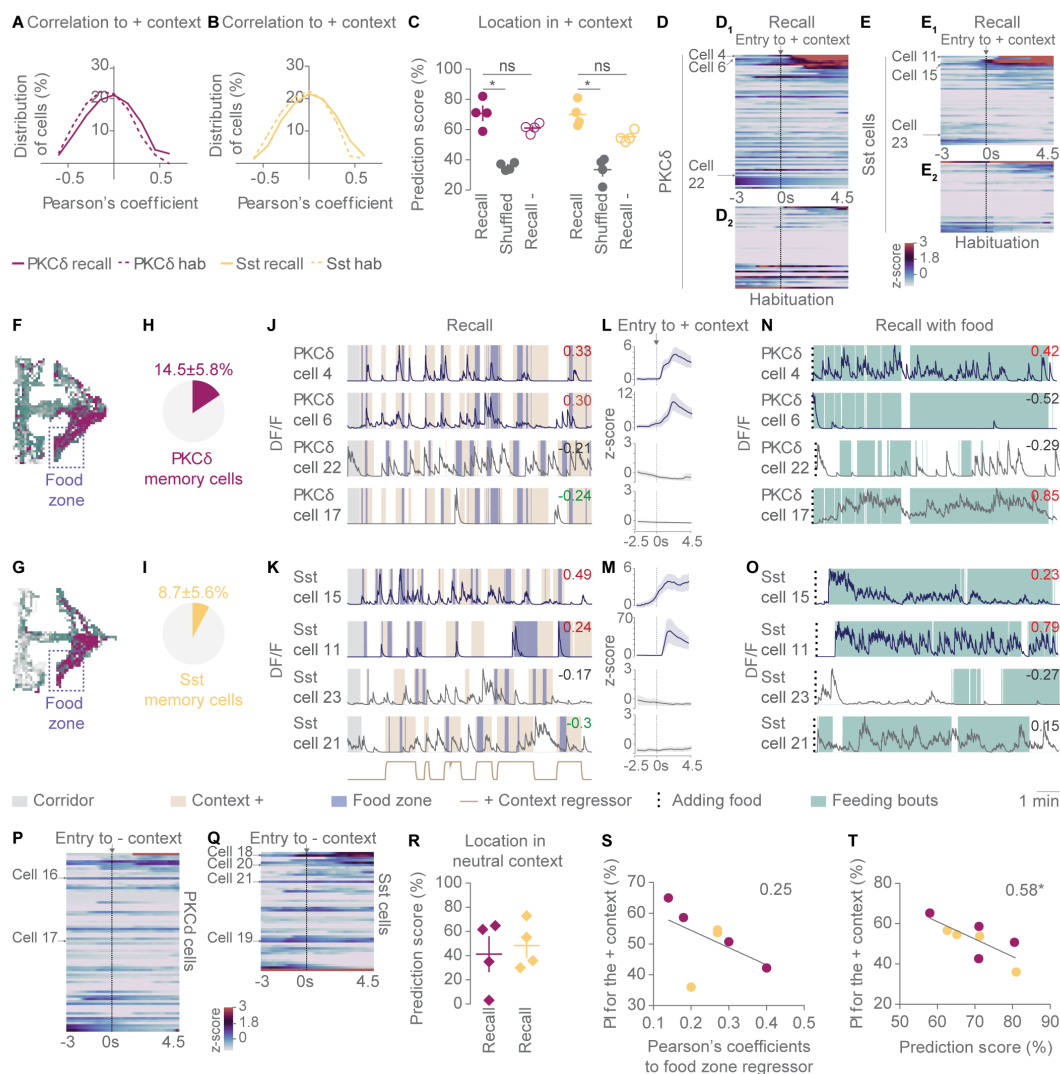


Figure 6

